Chemical Science

ROYAL SOCIETY OF CHEMISTRY

EDGE ARTICLE

View Article Online
View Journal | View Issue

Cite this: *Chem. Sci.*, 2026, **17**, 1232

All publication charges for this article have been paid for by the Royal Society of Chemistry

Exploring RNA G-quadruplex in the rabies virus genome and its potential against RABV infection

Xinying Zhang,†[ac] Geng Qin,†[b] Shengnan Lv,†[ad] Jianxiong Guo,[ac] Hualong Song,[e] Miles L. Postings,[e] Peter Scott,[e] Chunyu Wang,[f] Chuanqi Zhao,*[b] Changchun Tu,*[ac] Yan Liu*[ac] and Xiaogang Qu*[b]

Rabies virus (RABV) is a prototypical neurotropic RNA virus that can cause rabies with an almost 100% fatality rate. Despite great efforts having been made to identify an effective therapeutic target of rabies, the host factors involved in RABV infection and the underlying mechanisms remain poorly understood. There are no effective drug targets for human rabies to date. Therefore, a better understanding of rabies pathogenesis and exploring new targets for antiviral treatments are crucial and urgent. In this study, we identify the presence of G-quadruplex (G4) in the RABV genome and uncover a novel role of G4 in RABV infection, in which stabilization of G4 can suppress G protein translation and viral replication. By systematic screening of 10 pairs of triplex metallohelices (designated as M1–M10), we found that one enantiomer of a pair of glycoconjugated metallohelices (Λ-M10) has exceptional RABV G4-stabilizing ability. Further studies show that Λ-M10 exhibits potent antiviral activity against RABV by targeting viral RNA G4s while maintaining minimal cytotoxicity in RABV-infected cell lines. More interestingly, having a nanosized structure and glycoconjugated modifications, M10 could cross the blood–brain barrier, supporting the potential in clinical therapy for RABV infection. Our findings elucidate the presence of G4 in the RABV genome, which can be targeted by G4 ligands such as metallohelices to suppress crucial G protein translation and viral replication, a previously unrecognized mechanism against RABV infection.

Received 13th June 2025
Accepted 5th November 2025

DOI: 10.1039/d5sc04344a

rsc.li/chemical-science

Introduction

Rabies is a deadly neurotropic disease with an almost 100% fatality rate, leading to around 59 000 deaths worldwide each year.[1,2] Rabies virus (RABV) is the causative agent of rabies and has a broad host range, including dogs, foxes, bats and other mammals. Up to now, vaccination in wild animals, especially in stray dogs, is the most effective strategy to control rabies.[3–5] People who are at risk of exposure or have been bitten by infected animals should promptly receive vaccination and post-exposure prophylaxis (PEP), particularly in cases of Category III exposure; nevertheless, death is inevitable once the above treatments fail to block the onset of clinical symptoms.[2] Numerous studies have revealed several receptors and potential targets of RABV infection and pathogenesis, such as neuronal cell adhesion molecule (NCAM),[6] p75 neurotrophin receptor (p75NTR),[7] and metabotropic glutamate receptor subtype 2 (mGluR2),[8] but there are no effective drug targets for human rabies to date. Therefore, a better understanding of rabies pathogenesis and exploring new concepts for antiviral treatments are still urgent and significant.

RABV is a single-stranded negative-sense RNA virus, classified within the Lyssavirus genus within the Rhabdoviridae family. The genome is approximately 12 000 bp and encodes five proteins: nucleoprotein (N), phosphoprotein (P), matrix protein (M), glycoprotein (G), and the viral RNA polymerase large protein (L). N protein encapsulates the viral genome and forms an N-RNA complex for the purpose of genome protection.[9] P and L proteins form the ribonucleoprotein (RNP) with N-RNA complex and play an important role in viral genome transcription and translation.[10] G protein forms spikes on the viral envelope, which recognize the cell receptors, and is also involved in assembly and budding. The M protein connects the nucleocapsid with the envelope and helps in constructing a compact viral particle.[11]

G-quadruplex (G4) is a non-canonical nucleic acid secondary structure, which is formed in guanine-rich (G-rich) strands by

[a]*Changchun Veterinary Research Institute, Chinese Academy of Agricultural Sciences, Changchun, Jilin, China. E-mail: liu820512@163.com; changchun_tu@hotmail.com*

[b]*Laboratory of Chemical Biology and State Key Laboratory of Rare Earth Resource Utilization, Changchun Institute of Applied Chemistry, Chinese Academy of Sciences, Changchun, Jilin, China. E-mail: xqu@ciac.ac.cn; zhaocq@ciac.ac.cn*

[c]*World Organization for Animal Health (WOAH) Reference Laboratory for Animal Rabies, Changchun, Jilin, China*

[d]*Department of Hepatobiliary and Pancreatic Surgery, General Surgery Center, The First Hospital of Jilin University, Changchun, Jilin, China*

[e]*Department of Chemistry, University of Warwick, Coventry CV4 7AL, UK*

[f]*State Key Laboratory of Supramolecular Structure and Materials, Jilin University, Changchun, Jilin 130012, China*

† These authors contributed equally.

Hoogsteen bonds. G4s have been identified in the genomes of a wide range of species and serve diverse biological functions.[12] In addition to being recognized as potential therapeutic targets for cardiovascular diseases, cancers, and neurodegenerative disorders such as amyotrophic lateral sclerosis, frontotemporal dementia, and Alzheimer's disease,[13,14] G4s have also been acknowledged as promising antiviral targets against various viruses, such as Epstein–Barr virus (EBV),[15] severe acute respiratory syndrome coronavirus-2 (SARS-CoV-2),[16] human immunodeficiency virus type 1 (HIV-1),[17] and Zika virus (ZIKV).[18] Moreover, the classic G4 ligands, such as TMPyP4, BRACO-19 and PDP, exhibit specific affinity towards G4s and demonstrate potential antiviral activity against various viruses mentioned above. For instance, TMPyP4 effectively inhibits the replication of HIV-1, hepatitis C virus, herpes simplex virus 1 (HSV-1), Kaposi's sarcoma-associated herpesvirus, ZIKV, and SARS-CoV-2.[19] However, the formation of RNA G4s in the context of RABV infection and their potential as therapeutic targets for rabies remain to be elucidated.

Compared with conventional small molecules, chiral triplex cationic metallohelices exhibit high positive charge and nanosized architectures and have diameters similar to those of short α-helical peptides.[20–23] This endows them with the ability to recognize a range of biological macromolecules, such as diversified DNA secondary structures and Alzheimer's disease-associated Aβ proteins.[24–26] Recently, metallohelices have been proven to be attractive G4 binders. More and more studies have displayed their great potential for a range of biomedical applications, including excellent anticancer activity and antimicrobial activity.

In this study, we reveal the presence of G4 structures in the RABV genome and systematically elucidate their functional significance in viral infection and pathogenesis. Specifically, the RNA G4, located in the open reading frame (ORF) of the CVS-11 G gene, was found to exert inhibitory effects on viral translation. Through screening of 10 pairs of antiviral chiral triplex metallohelices (M1–M10), we identified a glycoconjugated metallohelix enantiomer (Λ-M10) with exceptional RABV G4-stabilizing activity (Scheme 1). Compared with Δ-M10, Λ-M10 exhibited potent anti-RABV effects by selectively targeting viral RNA G4 structures while showing minimal cytotoxicity in infected cell lines. The inhibition effect is better than that of isoprinosine (IPS, also called inosine pranobex, a reported effective anti-rabies drug). Notably, due to its nanosized structure and glycoconjugated modifications, M10 can cross the blood–brain barrier (BBB), highlighting its therapeutic potential for clinical RABV treatment. Our findings uncover a previously unrecognized mechanism in RABV infection, establishing G4 as a promising antiviral target and underscoring the therapeutic potential of metallohelices in combating rabies.

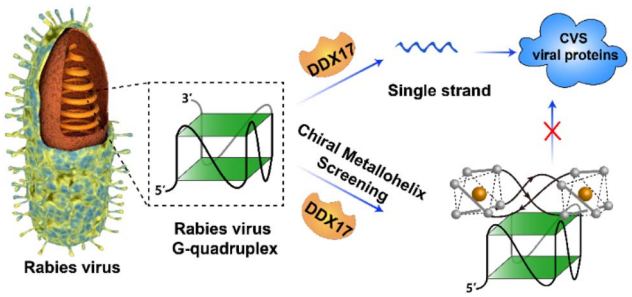

Scheme 1 G4s in RABV virus were verified as potential drug targets for anti-RABV therapy and glycoconjugated metallohelices exhibiting exceptional RABV G4-targeting.

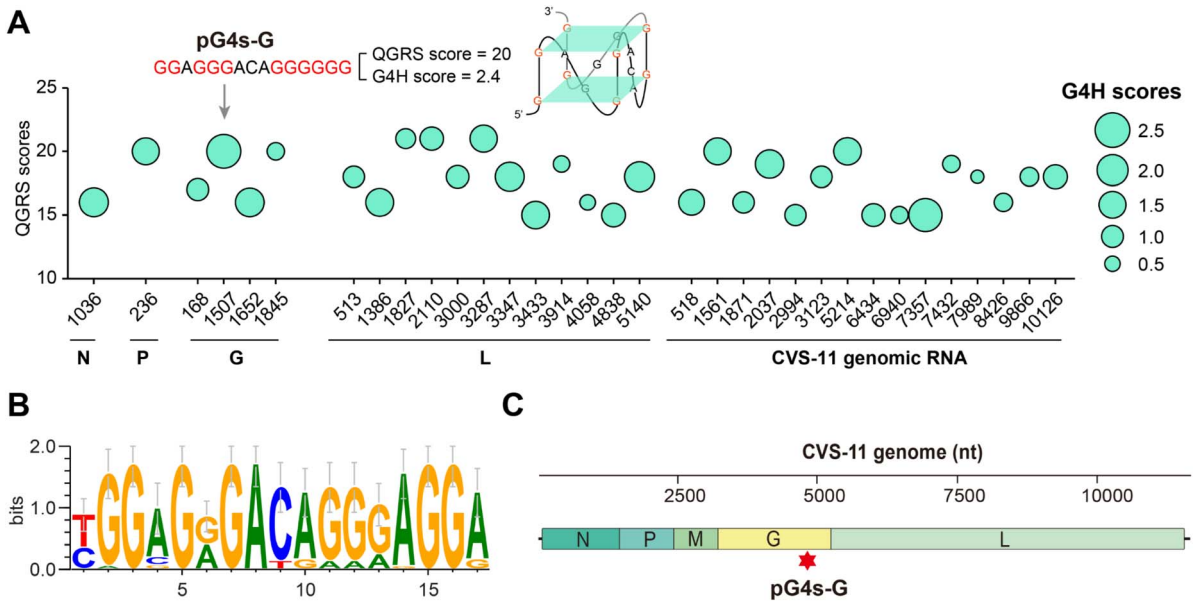

Fig. 1 Bioinformatics analysis and identification of G-quadruplexes (G4s) in the RABV genome. (A) The location and score of the rabies virus (RABV) putative G4 sequences (PQSs). The QGRS and G4H score of RABV PQSs calculated by G4 Hunter. (B) The analysis of conservation of the PQS candidates across strains by using WebLogo 3 software. (C) The location of pG4s-G in the genome of CVS-11.

Results

To explore the potential involvement of G4s in RABV, we initially screened all the putative G4-forming sequences (PQS) in the RABV genome by using a G4 analysis online platform and the challenge virus standard (CVS)-11 reference genome obtained from the NCBI database. As demonstrated in Fig. 1A, putative G4 sequences (PQS) were identified on both positive and negative strands of the CVS-11 genome, with 18 PQS located on the positive strand and 15 PQS located on the genomic RNA. The G4 folding capability of these PQS was evaluated by the putative Quadruplex forming G-Rich Sequences (QGRS) and G4 Hunter (G4H) scores (Fig. 1A and Table S1).

One of the PQS in the G gene of the positive strand exhibited a significantly high score in the analyses and was noted as pG4s-G. We next analyzed the conservation of this RABV G4 site by using WebLogo 3 software across 30 randomly selected RABV strains from the NCBI database. As demonstrated in Fig. 1B and S1, pG4s-G is conserved in diverse RABV strains. The location of pG4s-G in the CVS-11 genome is illustrated in the schematic diagram (1507–1521) (Fig. 1C). Together, the analyses indicated the presence of G4 in the RABV genome, and the top PQS (pG4s-G), which is the most stable one among 33 PQSs, was chosen for further experimental verification.

We employed several experiments to confirm the G4 formation of our candidate RABV-G4 sequence. The RNA oligo pG4s-G wild-type (pG4s-G-WT) and pG4s-G mutant (pG4s-G-Mut, with G/A mutations) were synthesized (Fig. 2A). We first examined the stability of pG4s-G-WT *in vitro* by *N*-methyl mesophorphyrin IX (NMM), a highly selective ligand for G4s, which is usually used as a fluorescent probe for G4 detection.[27] The data demonstrated that pG4s-G-WT significantly enhanced the NMM fluorescence in K^+ buffer (Fig. 2B). In contrast, pG4s-G-Mut showed a slight fluctuation in fluorescence intensity, suggesting the capability for G4 formation of this pG4s-G *in vitro*. The results were further supported by ThT fluorescence turn-on assays (Fig. S2). We then observed that pG4s-G-WT migrated faster than pG4s-G-Mut in electrophoresis. As nucleic acids with different secondary structures migrate at different speeds in the electrical field, this result indicates that a more compact structure was formed in pG4s-G-WT (Fig. 2C). The pG4s-G-WT exhibited similar migration rates to NS5-B M1 G4, a previously reported intramolecular G4, indicating that RABV G4 is an intramolecular G4.[28] This result was further confirmed by concentration-independent melting experiments (Fig. S3). Moreover, circular dichroism (CD) spectroscopy was performed to clarify the conformation of pG4s-G-WT, indicating that pG4s-G-WT formed parallel G4s with a typical negative peak around 240 nm and a positive peak around 262 nm. CD measurements showed that pG4s-G-WT rather than pG4s-G-Mut could form G4s (Fig. 2D). In brief, these results indicated that pG4s-G could form stable unimolecular G4s. Meanwhile, ^{1}H nuclear magnetic resonance (NMR) results showed that the spectrum of pG4s-G-WT had obvious peaks in the chemical shift region of G4s (Fig. 2E), further supporting the proposal that pG4s-G-WT can fold into a G4 structure. The RABV G4 formation *via* kinetic processes was analyzed by stopped-flow assays, which showed that the fluorescence intensity did not increase at 3.1 s, indicating that RABV G4 was completely formed within that time (Fig. 2F).

Immunostaining was further performed to identify G4 formation in RABV-infected cells. We used a classic G4-specific antibody, BG4, to facilitate the visualization of RNA G4s within the cytoplasm. BG4 is a monoclonal single-chain antibody that can specifically bind to DNA/RNA G4 structures with high affinity.[29] The recombinant RABV CVS-11-eGFP was used to present the colocalization of G4 with virus.[30] The result indicated that RABV replication led to the generation of a substantial quantity of viral G4, surpassing the cellular G4 levels. As G4 could be identified in the cell genome, the uninfected cells dyed with BG4 showed a faint red fluorescence. The infected cells, which could express the GFP-reporter gene, showed a significantly enhanced red fluorescence compared to the uninfected cells (Fig. 2G). Collectively, pG4s-G-WT could form a stable G4 *in vitro* and considerable G4s could form in the RABV infection process.

Along with illustrating G4 structures and biological functions, more hypotoxic and matched ligands were designed and synthesized to stabilize the formation of G4s. Compared with conventional small molecules, barrel-like metallohelices, available with a range of structures and functionalities, exhibit high positive charge and nanosized architectures, reminiscent of short α-helical peptides. According to our previous studies, metallohelices have been proven to be a new class of G4 binders. Herein, the binding of 10 pairs of iron triplex metallohelices to RABV-G4s was evaluated (Fig. S4 and S5). By conducting a fluorescent thermal melting assay (Fig. S6–S7 and 2H), we found that, among the 10 pairs of metallohelices, one glycoconjugated metallohelix enantiomer (M10) could significantly enhance the thermal stability of F-pG4s-G-WT-T (pG4s-G-WT labeled with FAM and TAMRA) (Fig. 2I–J and S8–S10). NMM displacement assays indicated that Λ-M10 and Δ-M10 could employ a stacking mode with the G-quartet plane of RABV G4 (Fig. S11). Interestingly, compared with Δ-M10, Λ-M10 showed a stronger stabilizing effect when binding to RABV G4. Given that RABV adopts a right-handed G4 structure, we speculate that this configuration may exhibit higher compatibility with the helical structure of Λ-M10, leading to its stronger binding affinity than that of Δ-M10.

Noting that pG4s-G is located in the ORFs of the CVS-11 G gene, which is an essential component of viral particles, we then examined whether the formation of pG4s-G could inhibit the translation of G proteins. The 18-base-pair sequences of pG4s-G-WT and pG4s-G-Mut were cloned into the N terminus of eGFP reporter gene on pcDNA3.1-eGFP vector (Fig. 3A). The plasmids were then transfected into HEK-293 cells to detect the protein expression. The results showed that the pG4s-G-WT plasmid expressed less eGFP than pG4s-G-Mut, indicating that the G4 formation interfered with the protein biosynthesis process in cells (Fig. 3B). Subsequently, we further explored the effects of Δ-M10 and Λ-M10 on protein expression by immunofluorescence assay. As demonstrated in Fig. 3C, the fluorescence intensity indicated that Δ-M10 and Λ-M10 inhibited the expression of eGFP as compared with the control group in pG4s-

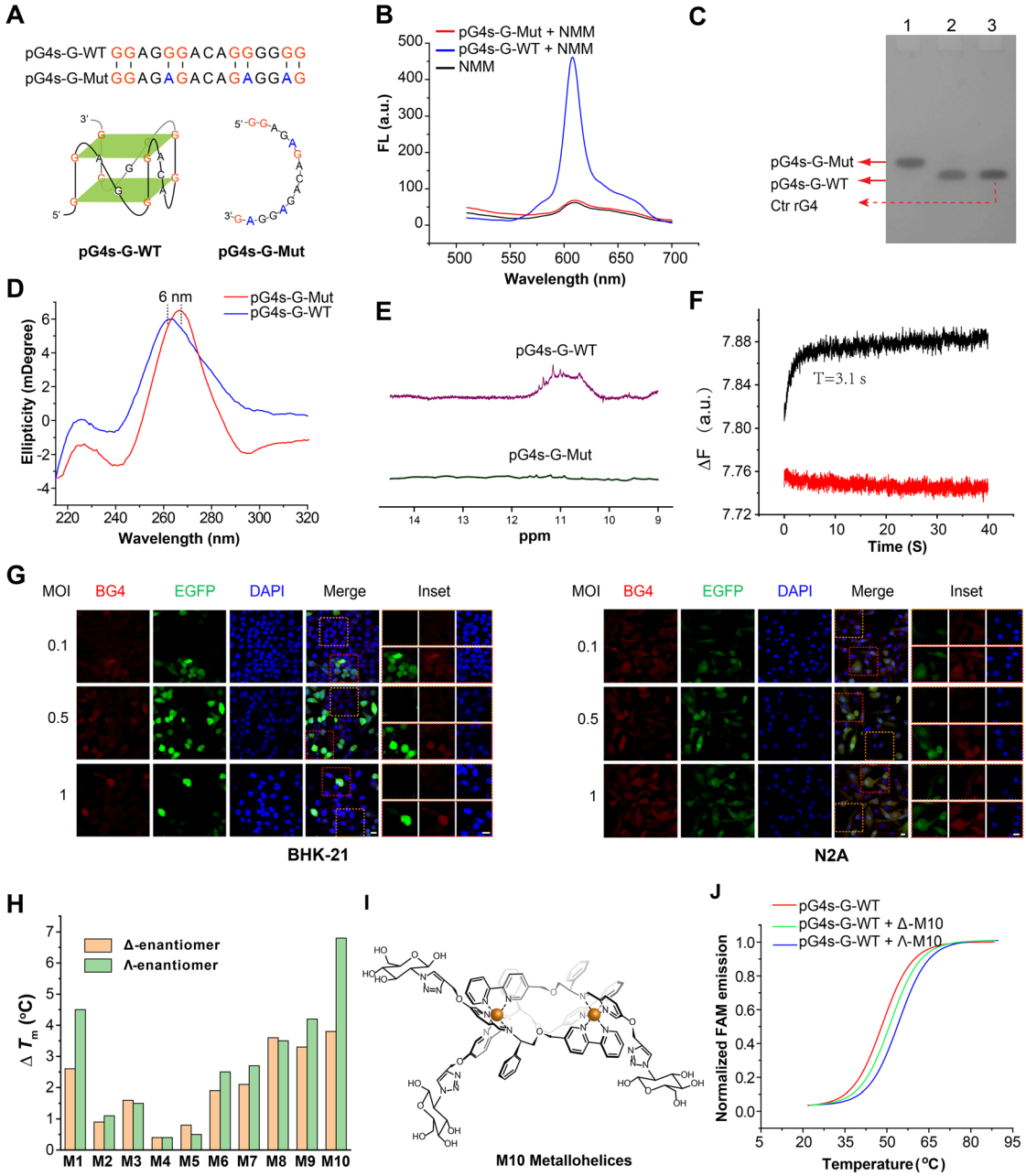

Fig. 2 Characterization of P4 G4 formation. (A) The sequences and schematic structures of pG4s-G-WT and pG4s-G-Mut. (B) NMM fluorescence turn-on assays in the absence or presence of pG4s-G-WT and pG4s-G-Mut. (C) The G4 formation of pG4s-G analyzed by gel studies. Lane 1, pG4s-G-WT; lane 2, pG4s-G-Mut; lane 3, control RNA G4 (NS5-B M1 G4). (D) CD spectra of pG4s-G-WT and pG4s-G-Mut. (E) ^{1}H NMR spectra of pG4s-G-WT and pG4s-G-Mut. (F) Stopped-flow traces of pG4s-G-WT and pG4s-G-Mut samples treated with buffer containing 200 mM [K^{+}]; excitation wavelength was 492 nm, data recorded at 578 nm. (G) The formation of G4s in RABV-infected cells detected by immunofluorescence assays in BHK-21 and N2A at different MOI. Left, CVS-11-EGFP infected BHK-21 (green), BG4-visualized G4s (red) and DAPI (blue); right, the same experiments in N2A. The red square indicates the uninfected cell, and the yellow square indicates the infected cell. MOI, multiplicity of infection. (H) Stabilization of RABV G4 by metallohelices M1–M10 in K^{+} buffer. (I) The chemical structures of M10. (J) Fluorescent thermal melting curves of pG4s-G-WT (0.5 μM) with the addition of Δ-M10 (0.5 μM) and Λ-M10 (0.5 μM).

G-WT transfected cells, while the fluorescence intensity was not influenced by either Δ-M10 or Λ-M10 in pG4s-G-Mut transfected cells. Western blot also showed consistent results: the protein expression of pG4s-G-WT, but not pG4s-G-Mut, was significantly inhibited by Δ-M10 and Λ-M10 in a dose-dependent manner. As expected, the inhibition of Λ-M10 was greater than that of Δ-M10 (Fig. 3D). Meanwhile, the KRAS-G4 vector, as a negative control, was transfected into HEK-293T cells and treated with Δ-M10 or Λ-M10, as shown in Fig. 3E and F, Neither Δ-M10 nor Λ-M10 downregulated the level of KRAS-G4, indicating that the enantiomer indeed had selectivity over cellular G4s.

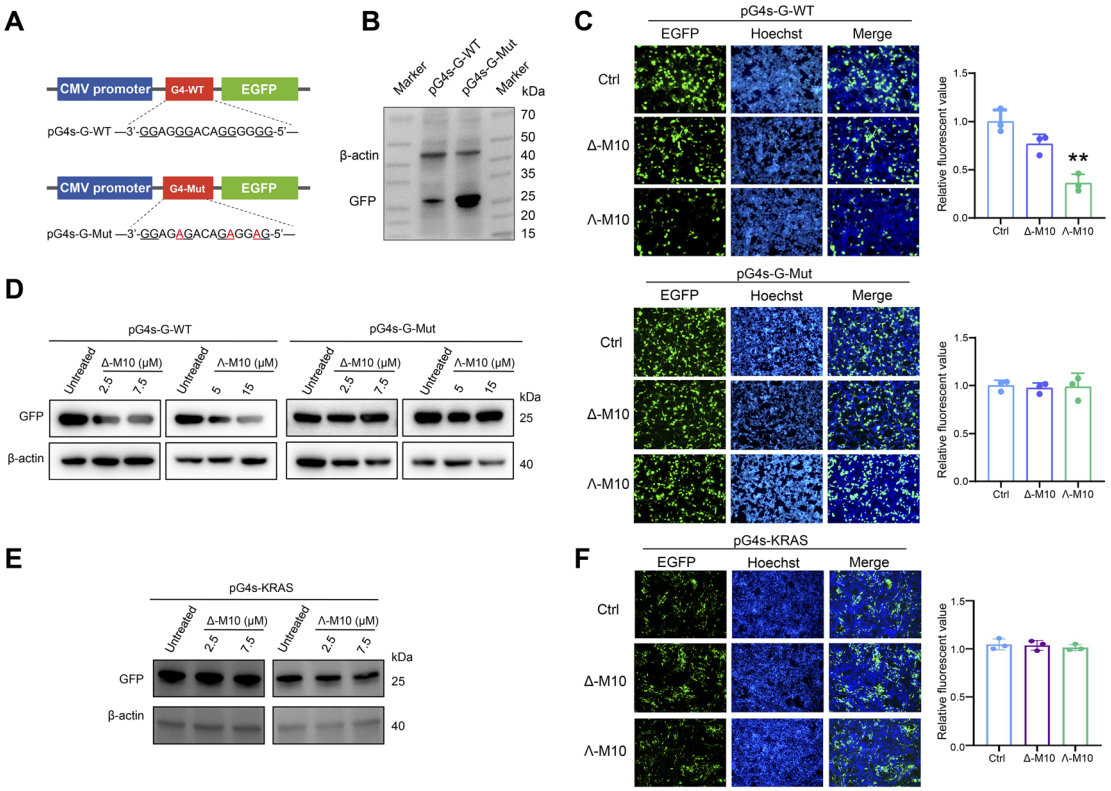

Fig. 3 Formation of pG4s-G G4 inhibits RABV RNA translation. (A) Schematic representation of the vector. The vectors were engineered to harbor 18 bp of the target pG4s-G G4s. Top, the sequences of pG4s-G-WT; bottom, pG4s-G-Mut. Bottom, schematic representation of the proposed pG4s-G-WT and pG4s-G-Mut structures. (B) The formation of pG4s-G G4 inhibits the translation of RNA with pG4s-G G4. (C) HEK293 cells transfected with pG4s-G-WT, pG4s-G-Mut and pG4s-KRAS (DNA G4) were treated with Δ-M10 or Λ-M10, followed by staining of the cell nuclei with Hoechst dye. The fluorescence microphotographs of the same cells with GFP (left), Hoechst (middle) or merge (right) are demonstrated. Quantitative analysis of fluorescence intensity was performed. (D) Western blotting assay was used to detect the protein expression, with β-actin as control. (E and F) HEK293 cells were transfected with pG4s-KRAS and then treated with Δ-M10 or Λ-M10. Western blotting assay was used to detect the expression of GFP-G4s-KRAS, with β-actin as control. The cell nuclei were stained with Hoechst dye. The fluorescence microphotographs of the same cells with GFP (left), Hoechst (middle) or merge (right) are demonstrated (E). Quantitative analysis of fluorescence intensity was performed (F).

Taken together, these results indicate that the formation of pG4s-G suppresses the translation process during the viral life cycle. Notably, Δ-M10 and Λ-M10 enantiomers displayed chirality-dependent activity, with Λ-M10 demonstrating superior binding affinity and translation inhibition.

To evaluate the therapeutic potential of Λ-M10, we examined its binding selectivity for RABV RNA G4s in the presence of various DNA and RNA G4s in the host. We performed FRET melting competitive assays of F-pG4s-G-WT-T and employed 10 unlabeled DNA G4s and 7 RNA G4s as competitors (Table S2). The results revealed that, even with a 3-fold excess of competing G4s, the T_m of the Λ-M10/F-pG4s-G-WT-T complex decreased only moderately, suggesting that host-derived DNA and RNA G4s weakly interfere with the binding of Λ-M10 to pG4s-G-WT (Fig. S12). Under these competitive conditions, Λ-M10 still binds effectively to RABV G4s, as evidenced by an increase in melting temperature (ΔT_m > 4 °C), indicating that Λ-M10 retains its ability to bind RABV G4s even in the presence of various host G4 structures. Moreover, after RABV infection, viral replication would generate abundant RABV G4s, the levels of which substantially exceed those of endogenous RNA/DNA G4s. This amplification of viral G4s would offset the binding specificity issue of Λ-M10 toward RABV G4s, thereby considerably reducing the off-target effects.

To evaluate the antiviral effects of Λ-M10 and Δ-M10 in RABV infection, we measured the intracellular viral RNA copies, protein levels, and viral titers in the supernatant of CVS-11 infected-N2A cells. IPS was used to act as a positive control; IPS is an immunomodulatory drug approved in several countries for the treatment of viral infections and has been proven to be effective in inhibiting RABV replication in our previous studies.[31]

As shown in Fig. 4A, both Λ-M10 and Δ-M10 significantly decreased the intracellular viral RNA copies in a dose-dependent manner, the effect of Λ-M10 being better than that of Δ-M10. More importantly, their antiviral effects were better than that of IPS. Consistent with the intracellular RNA copies, the virus titers in cell supernatant were remarkably reduced by Λ-M10 as compared with IPS by a maximal $\sim 3 - \log_{10}$ *vs.* $\sim 1 - \log_{10}$ (Fig. 4B). Meanwhile, we also found that the expression level of intracellular viral N protein was also reduced by all three treatments in a dose-dependent manner (Fig. 4C). In addition,

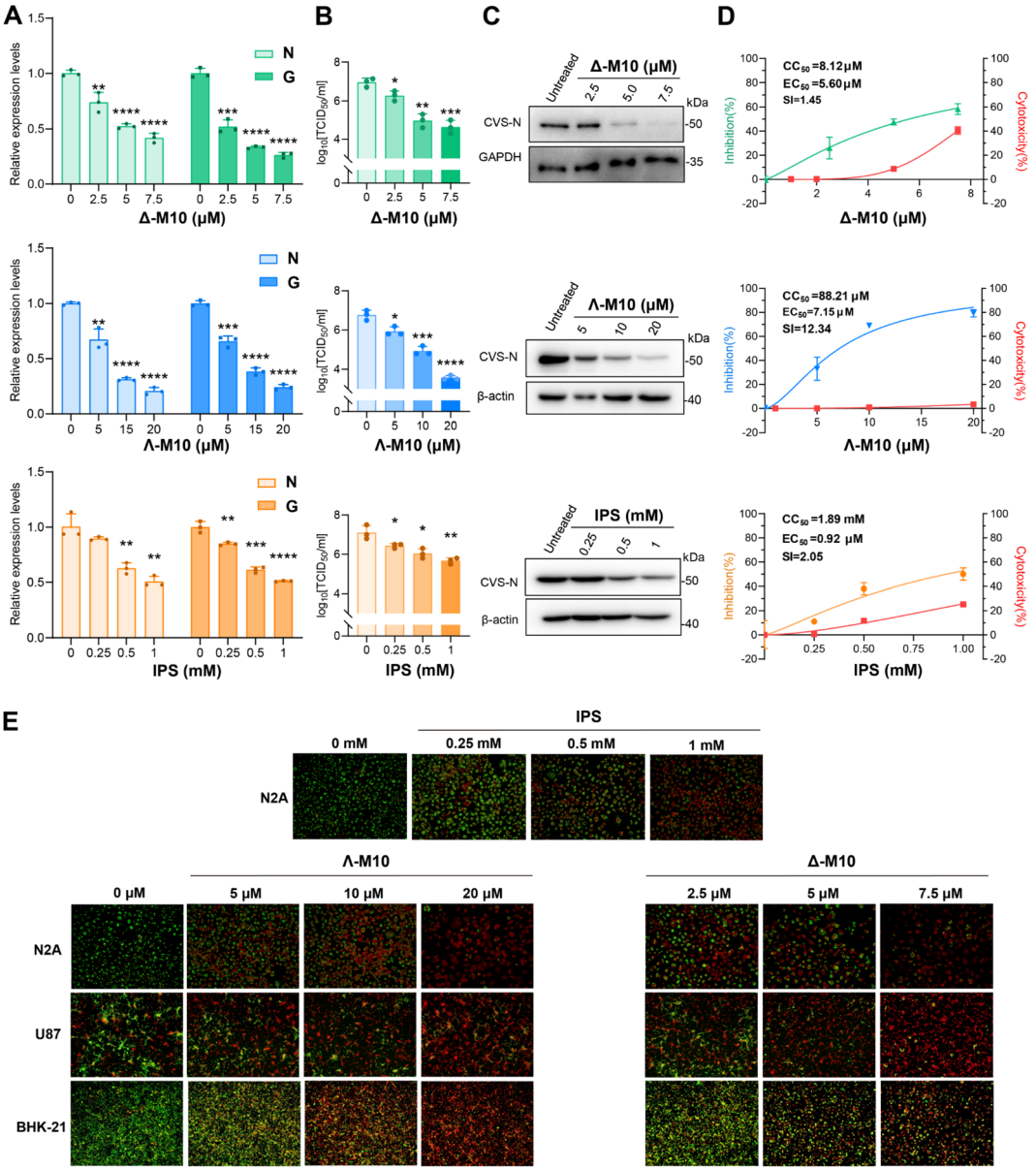

Fig. 4 Anti-RABV experiments of Λ-M10 in infected cells (A–C). N2A cells infected with CVS-11 (MOI = 0.1) were treated with Δ-M10, Λ-M10 or IPS pre-infection. At 48 h post-infection, viral N gene and G gene RNA copies in cell lysates (A) were detected by qRT-PCR. Viral N protein expression (B) was detected by WB. Viral titers (log_{10} $TCID_{50}$/mL) of cell culture supernatants (C) were quantified by $TCID_{50}$. (D) Intracellular viral RNA copies and cell viability under increasing concentration of different compounds to determine the EC_{50} and CC_{50} of Δ-M10, Λ-M10 and IPS. The drug cytotoxicity was determined by SRB assays. EC_{50}, half-maximal effective dose; CC_{50}, half-cytotoxic concentration; SI = CC_{50}/EC_{50}. Data are shown as means ± SEM of three independent experiments, two-tailed student's *t*-test. $^{**}P < 0.01$, $^{***}P < 0.001$, $^{****}P < 0.0001$. (E) Direct fluorescent assay with infected N2A, U87 and BHK-21. The viral particles were visualized by FITC anti-Rabies monoclonal globulin (green). The cells were dyed with evans blue (red).

half-cytotoxic concentration (CC_{50}), half-maximal effective dose (EC_{50}) and selectivity index (SI) of the three compounds were determined. Compared with Δ-M10 (CC_{50} = 8.12 μM, EC_{50} = 5.60 μM, SI = 1.45) and IPS (CC_{50} = 1.95 mM, EC_{50} = 0.33 mM, SI = 5.85), Λ-M10 (CC_{50} = 88.21 μM, EC_{50} = 7.15 μM, SI = 12.34) exhibited a lower cytotoxicity and a higher SI (Fig. 4D). The similar antiviral efficiency of Λ-M10 was further confirmed in baby hamster kidney-21 (BHK-21) cells, which are the most susceptible cells for RABV infection (Fig. S13).

We next performed a direct fluorescent antibody (DFA) assay to visualize the antiviral effect of Λ-M10 on RABV-susceptible cell lines. As demonstrated in Fig. 4E, the virus developed a green fluorescence, and cells were stained red with Evans Blue. The antiviral effects of Λ-M10 and Δ-M10 were obvious, although the cytotoxicity of Δ-M10 was a little higher, both of them exhibiting better anti-RABV efficacy than IPS, while a similar function was not observed in other metallohelices (Fig. S14). Collectively, these results suggest that Λ-M10 shows an outstanding dose-dependent antiviral effect in several RABV-

susceptible cell lines with lower cytotoxicity and higher SI, as compared to IPS and Δ-M10.

To confirm the acting targets of G4 ligands in RABV-infected cells, antisense oligonucleotides (ASOs), which can specifically unfold the G4s structure, and the random control oligo were designed and synthesized (Fig. 5A). ASOs were pre-transfected into N2A cells 12 hours prior to CVS-11 infection, and the unfolded G4s, which were probed by ASOs, would not be recognized by the antiviral compounds. As indicated in Fig. 5B, the antiviral effects of both Λ-M10 and Δ-M10 were antagonized by ASOs, confirming that these antiviral compounds indeed interfered with viral replication by specifically targeting G4s in the viral genome.

To further identify the acting phases of Λ-M10 in RABV infection, we conducted a time-of-addition assay and determined the viral titers in cell culture supernatant. The compounds were added at the indicated time points, and acted for diverse periods (Fig. 5C). The results demonstrated that the viral titers were significantly inhibited by Λ-M10 and Δ-M10 at a stage after viral entry, consistent with their putative antiviral mechanism by targeting viral G4s. It is worth noting that the treatment time is important for the function of the compounds. Neither pretreatment for 1 hour nor being incubated with virus for 1 hour had an antiviral effect, while the post-infection treatment following 48 hours of incubation showed a significant inhibitory effect, the same as the full-time inoculation (Fig. 5D). Meanwhile, the intracellular N gene expression at both mRNA and protein levels was significantly suppressed in Λ-M10-treated groups, after infected with CVS-11 for 48 hours no matter pretreated for 1 hour or not (Fig. 5E and F).

Similar results were also observed in the DFA assay. Very limited fluorescence reflected the satisfactory antiviral effect of Λ-M10 treatment (Fig. 5G). In addition, Δ-M10 also showed an acceptable antiviral effect; however, noting its cytotoxicity, Λ-M10 was the better choice for anti-RABV. Taken together, Λ-M10 was identified as an effective anti-RABV compound by targeting G4s and suppressing viral replication.

Noting that the DEAH-box helicases usually unfold G4 structure on both RNA and DNA strands (37827695, 35194205), we performed RNA pulldown assay by biotin-labeled G4 probes and mass spectrometry in RABV-infected N2A cells as compared to uninfected cells. The results identified DDX17 significantly enriched in RABV-G4 pulldown samples (Table S2), and could interact with RABV-G4, but not RABV-G4-MUT (Fig. 6A and B). CD spectroscopy is usually used to characterize the conformational changes of G4 structures and the effect of proteins on the conformation of the G4s (35504902, 36043100). DDX17 is also known as ATP-dependent RNA helicase p72, activation of which could be suppressed by a K142R point mutation contained within the ATP-binding domain (12138182). To clarify the function of DDX17 on unfolding RABV-G4, we constructed DDX17-WT and DDX17-K142R overexpression vectors and purified their proteins to perform ATPase hydrolysis experiments (Fig. S15). The results indicated that the CD intensity at 260 nm of RABV-G4 significantly decreased with the addition of DDX17, which further slightly declined with the addition of ATP (Fig. 6C). These results suggest that DDX17 interacts with and impacts the RABV-G4 structure in an ATP-dependent manner.

We then examined the function of DDX17 alone and combined with Λ-M10 on regulating RABV replication by using western-blot and qPCR. The data indicated that DDX17 significantly promoted the replication of RABV, whereas Λ-M10 inhibited DDX17-mediated induction of CVS viral protein expression (Fig. 6D and E). In addition, the viral titers and replication were further measured by $TCID_{50}$ and DFA assays to clarify whether overexpressed DDX17 could diminish the function of Λ-M10, and consistent results were observed. DDX17 promoted RABV replication, while 20 μM Λ-M10 suppressed viral replication no matter with or without DDX17 overexpression (Fig. 6F and G). Taken together, DDX17 unwinds the RABV-G4 structure and promotes RABV replication, and Λ-M10 can overcome the function of DDX17.

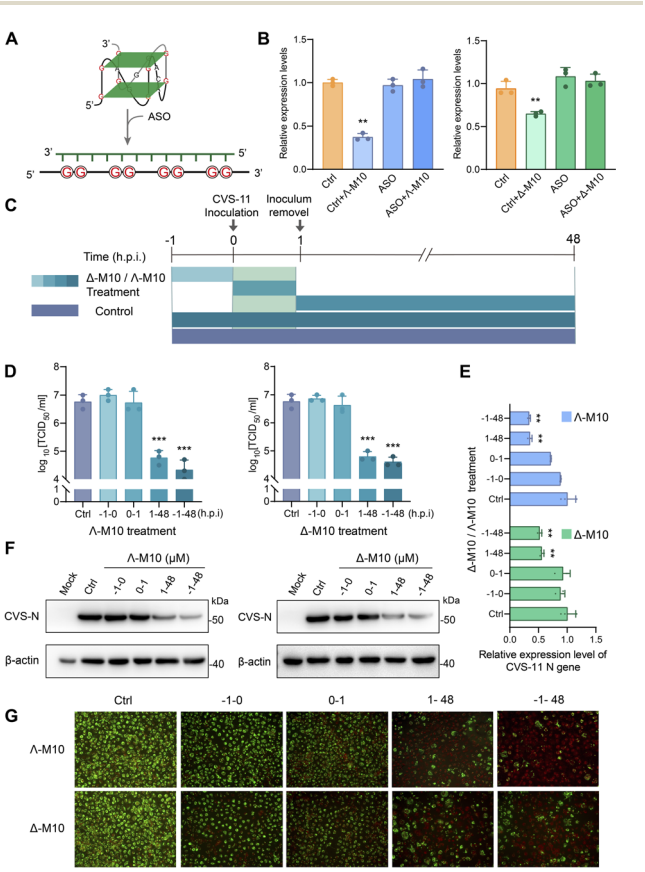

Fig. 5 Anti-RABV Λ-M10 inhibits RABV infection by targeting RABV-G4s. (A) Schematic representation of the antisense oligonucleotide treatment to probe and unfold viral G4 structures. (B) ASOs targeting pG4s-G were pre-transfected into N2A 12 h before virus infection and ligand addition. At 48 h post-infection, viral RNA copies in cell lysates were detected by qRT-PCR. (C–G) Time-of-addition assay of Λ-M10 and Δ-M10. The scheme illustrates the period of virus inoculation and ligand addition (C). N2A cells were incubated with 20 μM Λ-M10 or 7.5 μM Δ-M10 at the time points indicated. The cells were infected with CVS-11 (MOI = 0.1), and the cell culture supernatant viral titers (D), intracellular viral RNA copies (E) and viral N protein expression (F) were quantified by $TCID_{50}$, qRT-PCR and WB. The fluorescence micrographs in DFA are demonstrated (G). Data are shown as means ± SEM of three independent experiments, two-tailed student's *t*-test. $^{**}P < 0.01$, $^{***}P < 0.001$, $^{****}P < 0.0001$.

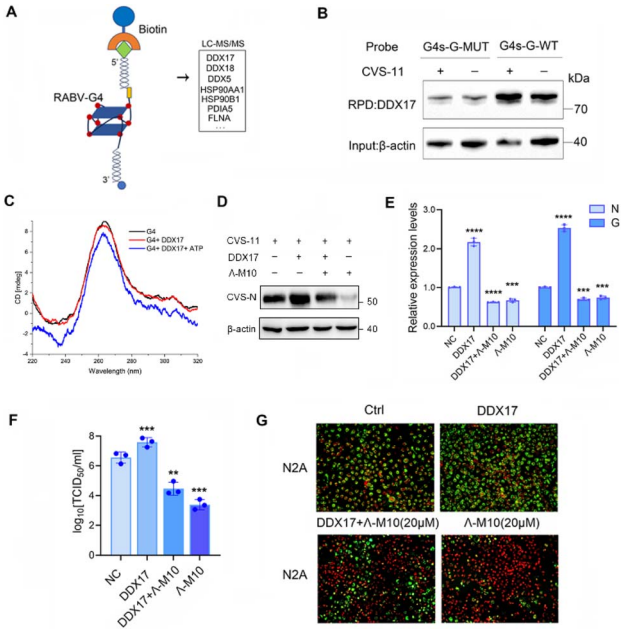

Fig. 6 Host DDX17 unfolds RABV-G4s and exogenous DDX17 decreases the function of RABV-G4 stabilizing agent Λ-M10. (A) Schematic diagram showing the process of RNA pulldown by RABV-G4 probes and detection of interacting proteins by LC-MS/MS. (B) N2A cells were infected with CVS-11 (MOI = 0.1) for 48 h, and RNA-pull-down assay was performed using RABV-G4 or RABV-G4-MUT probes. The level of pulldown DDX17 protein was detected by WB, with β-actin as control. (C) The effects of DDX17 on RABV-G4 structure in the absence or presence of ATP by CD spectral analysis. (D–G) N2A cells were transfected with DDX17-overexpression plasmid for 24 h and then infected with CVS-11 (MOI = 0.1). After that, the cells were treated with 20 μM Λ-M10 for 48 h and viral N protein expression level (D), viral N and G gene RNA copies in cell lysates (E), and viral titers in supernatants (F) were detected by WB, qRT-PCR and $TCID_{50}$. The fluorescence microphotographs in DFA are demonstrated (G). Data are shown as means ± SEM of three independent experiments, two-tailed student's *t*-test. $^{**}P < 0.01$, $^{***}P < 0.001$, $^{****}P < 0.0001$.

Discussion

Rabies is an ancient fatal zoonosis and still causes nearly 59 000 deaths globally each year. Unfortunately, there are no effective drugs for rabies therapy to date. Different kinds of drugs have been identified, such as BCX4430, PGG, deoxynivalenol (DON), TMR-001, pyrimethamine, artesunate (ART) and dihydroartemisinin (DHA), among which BCX4430 inhibits the replication of rabies virus by suppressing mTOR-dependent autophagy *in vitro*.[32] DON and favipiravir have a positive effect on inhibiting the replication of several viruses, including RABV.[33,34] Pyrimethamine has been shown to suppress RABV replication *in vitro* by targeting adenosine synthesis; however, its therapeutic potential is limited due to the lack of efficacy *in vivo*.[35] Artemisinin derivatives, particularly ART and DHA, demonstrate significant antiviral activity against RABV.[36] However, none of these drugs has been approved for rabies clinical treatment.

The positive-sense RNA viral genome functions as a dual-purpose template, facilitating both viral replication and translation processes. This unique characteristic results in the incorporation of numerous functional RNA elements that can actively regulate gene expression mechanisms independently of viral protein synthesis, thereby exerting control over host cellular machinery at the earliest stages of infection. Therefore, we tried to reveal the specific nucleic acid structures involved in the gene modulation in the RABV genome to elucidate groundbreaking anti-RABV mechanisms and innovative therapeutic drugs against rabies.

G4 is a novel antiviral target emerging in recent years, and the formation of G4s plays important roles in transcription, telomere biology and genome instability. Recent RNA G4 profiling analyses have identified thousands of putative RNA G4 regions in the human transcriptome,[37,38] strongly suggesting a causal role of this structural RNA element in multiple human diseases, such as cancer, neurodegenerative diseases and metabolic disorders.[39] Thus, G4 is emerging as a potential therapeutic target and many G4-specific ligands have been designed and utilized to stabilize G4s. TMPyP4, one of the G4 ligands, suppresses the expression of cellular-myelocytomatosis viral oncogene (*c*-MYC) by stabilizing G4s in its promoter.[40] CM03, another G4 ligand, can target many oncogenic pathways essential to tumorigenesis and exhibits an anticancer effect on human pancreatic ductal adenocarcinoma (PDAC) in a mouse xenograft model.[41] CX-3543 (Quarfloxin) and CX-5461 (Pidnarulex) inhibit the transcriptional activity of RNA polymerase by targeting G4. Both exhibit promising potential in anticancer therapy and have been tested in clinical trials.[42–44]

In this study, we identified 33 putative G4s in the reference genome of CVS-11 for the first time, and the top G4 sequence, pG4s-G, was selected as the candidate G4 for further study, which is also a highly conserved sequence in different RABV strains. We first confirmed that pG4s-G-WT could form a stable G4 *in vitro*, then a BG4 antibody and the recombinant RABV CVS-11-eGFP were used to further confirm that pG4s-G could also form G4 structure in the infection process. We then tried to find the specific ligands of pG4s-G.[45] By screening 10 pairs of triplex metallohelices, we identified one enantiomer of a pair of glycoconjugated metallohelices (Λ-M10) that has exceptional RABV G4-stabilizing ability. The primary experiment identified the affinity between the metallohelices and pG4s-G-WT, and the antiviral experiments demonstrated that both Λ-M10 and Δ-M10 could significantly inhibit the replication of RABV. Actually, we also identified another ligand (named NiM), but it is inefficient. Further study determined that Λ-M10 exhibited a more potent antiviral capacity than Δ-M10 and IPS with a much lower cytotoxicity. It is interesting that although the chiral ligands have similar structures, their cytotoxicity and pharmaceutical effects are quite different, which deserves further studies in the future.

Furthermore, we provided several lines of evidence, for the first time, to demonstrate that our Λ-M10 acts as a potential anti-RABV compound by targeting G4s in the context of RABV infection. The pG4s-G-WT and pG4s-G-Mut plasmids with eGFP reporter gene were transfected into HEK-293 cells, and Λ-M10 significantly inhibited the fluorescence intensity and the protein expression of eGFP in pG4s-G-WT transfected cells, but

not in pG4s-G-Mut transfected cells. We further pre-transfected ASOs into infected cells. The unfolded G4, which was probed by ASOs, would not be recognized by the antiviral compound Λ-M10. As expected, we observed that the antiviral effect of Λ-M10 was antagonized by ASOs, confirming that the antiviral compound Λ-M10 indeed interfered with viral replication by specifically targeting G4s in the viral genome. Moreover, the time-of-addition assay suggested that the inhibition function of Λ-M10 was effective mainly at a stage post-RABV entry by targeting viral G4s.

Meanwhile, it should be noted that G4s also exist in the DNA and mRNA of host cells and are involved in many biological processes. Just like other G4-specific stabilizers, the off-targeting of Λ-M10 could possibly cause side effects. Previous studies have proposed that viral particles may replicate rapidly in infected cells and produce a large amount of viral G4s, much more abundant than intracellular G4s,[46] such as the number of viral G4s increasing sharply in HSV-1 infected cells[47] and we previously reported that SARS-CoV-2 infected cells contain hundreds of copies of viral RNA G4 targets, being more numerous than cellular G4s.[16] Herein, a similar phenomenon was observed in RABV-infected cells. With BG4 incubation, the high-intensity red fluorescence in RABV-infected cells indicated that abundant viral G4s were synthesized. Thus, it is believed that the ligands would have a better chance of interacting with viral G4 rather than intracellular G4 and an appropriate concentration of G4 ligands could balance the antiviral efficiency and the side effects. Certainly, it is of importance in future investigations to develop gene-specific G4-targeting agents.

For further application in clinical therapy for RABV infection, these metallohelices must cross the BBB. To assess whether M10 can passively accumulate in the brain, we measured iron (Fe) levels in mouse cerebrospinal fluid (CSF) 6 h after intraperitoneal injection using ICP-MS. Notably, mice treated with M10 exhibited significantly higher Fe levels in the CSF compared to control mice. The brain accumulation efficiencies were 3.5% for Λ-M10 and 3.3% for Δ-M10, confirming their ability to traverse the BBB. These findings further support the potential of metallohelices as clinical therapeutic agents against RABV. Interestingly, unlike small molecules that typically exhibit limited BBB penetration, M10 may leverage its nanoscale size and glycoconjugated modifications to facilitate crossing. These structural features could enhance its therapeutic potential for central nervous system (CNS) infections.

Conclusion

In conclusion, this study demonstrates the presence of G4 structures in the RABV genome. Stabilizing RABV G4 formation could suppress G protein translation and inhibit viral replication. By screening 10 pairs of triplex metallohelices, we identified a glycoconjugated metallohelix enantiomer, Λ-M10, exhibiting potential anti-RABV effects by targeting viral RNA G4s while showing minimal cytotoxicity. Notably, due to its nanosized structure and glycoconjugated modifications, Λ-M10 can cross the BBB, highlighting its therapeutic potential for clinical RABV treatment. Our findings uncover a previously unrecognized mechanism in RABV infection, establishing G4 as a promising antiviral target and underscoring the potential of metallohelices in developing novel RABV therapeutics.

Conflicts of interest

There are no conflicts to declare.

Data availability

The data supporting this article have been included as part of the supplementary information (SI). Supplementary information: experimental detail, conservation analysis, supplemental figures and tables. See DOI: **https://doi.org/10.1039/d5sc04344a**.

Acknowledgements

This work was supported by the following grants: the National Natural Science Foundation of China (32273093, 31972720, 22377120, 22437006, 31902307), National Key Research and Development Program of China (2022YFD1800100), and the Jilin Province Science and Technology Development Plan Project (20210101130JC).

References

1 C. R. Fisher, D. G. Streicker and M. J. Schnell, *Nat. Rev. Microbiol.*, 2018, **16**, 241.
2 K. Hampson, L. Coudeville, T. Lembo, M. Sambo, A. Kieffer, M. Attlan, J. Barrat, J. D. Blanton, D. J. Briggs, *et al.*, *PLoS Neglected Trop. Dis.*, 2015, **9**, e0003709.
3 F. X. Meslin and D. J. Briggs, *Antiviral Res.*, 2013, **98**, 291.
4 S. C. Totton, A. I. Wandeler, J. Zinsstag, C. T. Bauch, C. S. Ribble, R. C. Rosatte and S. A. McEwen, *Prev. Vet. Med.*, 2010, **97**, 51.
5 A. R. Fooks, A. C. Banyard, D. L. Horton, N. Johnson, L. M. McElhinney and A. C. Jackson, *Lancet*, 2014, **384**, 1389.
6 M. I. Thoulouze, M. Lafage, M. Schachner, U. Hartmann, H. Cremer and M. Lafon, *J. Virol.*, 1998, **72**, 7181.
7 C. Tuffereau, J. Benejean, D. Blondel, B. Kieffer and A. Flamand, *EMBO J.*, 1998, **17**, 7250.
8 J. Wang, Z. Wang, R. Liu, L. Shuai, X. Wang, J. Luo, C. Wang, W. Chen, X. Wang, J. Ge, X. He, Z. Wen and Z. Bu, *PLoS Pathog.*, 2018, **14**, e1007189.
9 T. Masatani, N. Ito, Y. Ito, K. Nakagawa, M. Abe, S. Yamaoka, K. Okadera and M. Sugiyama, *Microbiol. Immunol.*, 2013, **57**, 511.
10 S. A. Harmon, E. N. Robinson, Jr. and D. F. Summers, *Virology*, 1985, **142**, 406.
11 T. Mebatsion, F. Weiland and K. K. Conzelmann, *J. Virol.*, 1999, **73**, 242.
12 D. Varshney, J. Spiegel, K. Zyner, D. Tannahill and S. Balasubramanian, *Nat. Rev. Mol. Cell Biol.*, 2020, **21**, 459.
13 A. Cammas and S. Millevoi, *Nucleic Acids Res.*, 2017, **45**, 1584.
14 J. Yang, G. Qin, J. Niu, Y. Wei, X. Li, C. Zhao, C. Wang, J. Ren and X. Qu, *Chem. Commun.*, 2023, **59**, 1078.

15 P. Murat, J. Zhong, L. Lekieffre, N. P. Cowieson, J. L. Clancy, T. Preiss, S. Balasubramanian, R. Khanna and J. Tellam, *Nat. Chem. Biol.*, 2014, **10**, 358.
16 G. Qin, C. Zhao, Y. Liu, C. Zhang, G. Yang, J. Yang, Z. Wang, C. Wang, C. Tu, Z. Guo, J. Ren and X. Qu, *Cell Discov*, 2022, **8**, 86.
17 E. Butovskaya, P. Solda, M. Scalabrin, M. Nadai and S. N. Richter, *ACS Infect. Dis.*, 2019, **5**, 2127–2135.
18 P. Majee, A. Pattnaik, B. R. Sahoo, U. Shankar, A. K. Pattnaik, A. Kumar and D. Nayak, *Mol. Ther. Nucleic Acids*, 2021, **23**, 691.
19 E. Ruggiero and S. N. Richter, *Nucleic Acids Res.*, 2018, **46**, 3270.
20 H. Song, S. J. Allison, V. Brabec, H. E. Bridgewater, J. Kasparkova, H. Kostrhunova, V. Novohradsky, R. M. Phillips, J. Pracharova, N. J. Rogers, S. L. Shepherd and P. Scott, *Angew. Chem., Int. Ed.*, 2020, **59**, 14677.
21 C. Zhao, H. Song, P. Scott, A. Zhao, H. Tateishi-Karimata, N. Sugimoto, J. Ren and X. Qu, *Angew. Chem., Int. Ed.*, 2018, **57**, 15723.
22 Z. Du, C. Liu, Z. Liu, H. Song, P. Scott, X. Du, J. Ren and X. Qu, *Chem. Sci.*, 2023, **14**, 506.
23 A. D. Faulkner, R. A. Kaner, Q. M. Abdallah, G. Clarkson, D. J. Fox, P. Gurnani, S. E. Howson, R. M. Phillips, D. I. Roper, D. H. Simpson and P. Scott, *Nat. Chem.*, 2014, **6**, 797.
24 M. Li, S. E. Howson, K. Dong, N. Gao, J. Ren, P. Scott and X. Qu, *J. Am. Chem. Soc.*, 2014, **136**, 11655.
25 D. E. Mitchell, G. Clarkson, D. J. Fox, R. A. Vipond, P. Scott and M. I. Gibson, *J. Am. Chem. Soc.*, 2017, **139**, 9835.
26 H. Song, S. J. Allison, V. Brabec, H. E. Bridgewater, J. Kasparkova, H. Kostrhunova, V. Novohradsky, R. M. Phillips, J. Pracharova, N. J. Rogers, S. L. Shepherd and P. Scott, *Angew. Chem., Int. Ed.*, 2020, **59**, 14677.
27 A. Kreig, J. Calvert, J. Sanoica, E. Cullum, R. Tipanna and S. Myong, *Nucleic Acids Res.*, 2015, **43**, 7961.
28 J. R. Terrell, T. T. Le, A. Paul, M. A. Brinton, W. D. Wilson, G. M. K. Poon, M. W. Germann and J. L. Siemer, *Nat. Commun.*, 2024, **15**, 5428.
29 G. Biffi, D. Tannahill, J. McCafferty and S. Balasubramanian, *Nat. Chem.*, 2013, **5**, 182.
30 X. Xue, X. Zheng, H. Liang, N. Feng, Y. Zhao, Y. Gao, H. Wang, S. Yang and X. Xia, *Viruses*, 2014, **6**, 1578.
31 Z. Tu, W. Gong, Y. Zhang, Y. Feng, Y. Liu and C. Tu, *Viruses*, 2018, **10**, 201.
32 Y. Xie, Y. L. Chi, S. Q. Liu and W. Y. Zhu, *Virology*, 2023, **585**, 21.
33 Q. Liu, Q. He and W. Zhu, *Int. J. Mol. Sci.*, 2023, **24**, 7793.
34 K. Yamada, K. Noguchi, T. Komeno, Y. Furuta and A. Nishizono, *J. Infect. Dis.*, 2016, **213**, 1253.
35 S. Rogee, F. Larrous, D. Jochmans, Y. Ben-Khalifa, J. Neyts and H. Bourhy, *Antiviral Res.*, 2019, **161**, 1.
36 J. Luo, Y. Zhang, Y. Wang, Q. Liu, J. Li, H. He, Y. Luo, S. Huang and X. Guo, *Virol. Sin.*, 2021, **36**, 721.
37 J. U. Guo and D. P. Bartel, *Science*, 2016, 353.
38 C. K. Kwok, G. Marsico, A. B. Sahakyan, V. S. Chambers and S. Balasubramanian, *Nat. Methods*, 2016, **13**, 841.
39 G. Liu, W. Du, H. Xu, Q. Sun, D. Tang, S. Zou, Y. Zhang, M. Ma, G. Zhang, X. Du, S. Ju, W. Cheng, Y. Tian and X. Fu, *J. Hepatol.*, 2020, **73**, 371.
40 A. Siddiqui-Jain, C. L. Grand, D. J. Bearss and L. H. Hurley, *Proc. Natl. Acad. Sci. U. S. A.*, 2002, **99**, 11593.
41 C. Marchetti, K. G. Zyner, S. A. Ohnmacht, M. Robson, S. M. Haider, J. P. Morton, G. Marsico, T. Vo, S. Laughlin-Toth, A. A. Ahmed, *et al.*, *J. Med. Chem.*, 2018, **61**, 2500.
42 D. Drygin, A. Siddiqui-Jain, S. O'Brien, M. Schwaebe, A. Lin, J. Bliesath, C. B. Ho, C. Proffitt, K. Trent, J. P. Whitten, J. K. Lim, D. Von Hoff, K. Anderes and W. G. Rice, *Cancer Res.*, 2009, **69**, 7653.
43 E. Sanij, K. M. Hannan, J. Xuan, S. Yan, J. E. Ahern, A. S. Trigos, N. Brajanovski, J. Son, K. T. Chan, O. Kondrashova, E. Lieschke, M. J. Wakefield, D. Frank, S. Ellis, C. Cullinane, J. Kang, G. Poortinga, P. Nag, A. J. Deans, K. K. Khanna, L. Mileshkin, G. A. McArthur, J. Soong, E. Berns, R. D. Hannan, C. L. Scott, K. E. Sheppard and R. B. Pearson, *Nat. Commun.*, 2020, **11**, 2641.
44 L. Ferret, J. G. Pol, A. Sauvat, G. Stoll, K. Alvarez-Valadez, A. Muller, J. Le Naour, F. Peyre, G. Anagnostopoulos, I. Martins, M. C. Maiuri, H. Wodrich, L. Guittat, J. L. Mergny, G. Kroemer and M. Djavaheri-Mergny, *Autophagy*, 2025, **21**, 2246.
45 Y. H. Wang, Q. F. Yang, X. Lin, D. Chen, Z. Y. Wang, B. Chen, H. Y. Han, *et al.*, *Nucleic Acids Res.*, 2022, **50**, D150.
46 A. Abiri, M. Lavigne, M. Rezaei, S. Nikzad, P. Zare, J. L. Mergny and H. R. Rahimi, *Pharmacol. Rev.*, 2021, **73**, 897.
47 S. Artusi, R. Perrone, S. Lago, P. Raffa, E. Di Iorio, G. Palu and S. N. Richter, *Nucleic Acids Res.*, 2016, **44**, 10343.